Acta Crystallographica Section A
Foundations of Crystallography
ISSN 0108-7673

Received 2 October 2009
Accepted 26 November 2009

Structural dynamics of photoinduced molecular switching in the solid state

Hervé Cailleau,[a]* Maciej Lorenc,[a] Laurent Guérin,[b] Marina Servol,[a] Eric Collet[a] and Marylise Buron-Le Cointe[a]

[a]Institut de Physique de Rennes, Université de Rennes1-CNRS, UMR 6251, F-35042 Rennes, France, and [b]European Synchrotron Radiation Facility, F-38043 Grenoble, France. Correspondence e-mail: herve.cailleau@univ-rennes1.fr

Fast and ultra-fast time-resolved diffraction is a fantastic tool for directly observing the structural dynamics of a material rearrangement during the transformation induced by an ultra-short laser pulse. The paper illustrates this ability using the dynamics of photoinduced molecular switching in the solid state probed by 100 ps X-ray diffraction. This structural information is crucial for establishing the physical foundations of how to direct macroscopic photoswitching in materials. A key feature is that dynamics follow a complex pathway from molecular to material scales through a sequence of processes. Not only is the pathway indirect, the nature of the dynamical processes along the pathway depends on the timescale. This dictates which types of degrees of freedom are involved in the subsequent dynamics or kinetics and which are frozen or statistically averaged. We present a recent investigation of the structural dynamics in multifunctional spin-crossover materials, which are prototypes of molecular bistability in the solid state. The time-resolved X-ray diffraction results show that the dynamics span from subpicosecond molecular photoswitching followed by volume expansion (on a nanosecond timescale) and additional thermoswitching (on a microsecond timescale).

1. Introduction

A current challenge in science and technology is to direct the functionality of matter at the relevant scale. Spectacular advances are made in nanoscience with the mastering of energy and information on the nanometre scale. Equally important is the tracking and control of dynamic processes in matter in ultra-short time. This feat can be accomplished thanks to the increase of sophisticated technologies and instrumentation, including time-resolved diffraction. They give fascinating capabilities not only to observe and understand the elementary dynamic processes in materials, chemistry and biology, but also to study how matter works and can be directed to a desired outcome. A great example is provided by femtochemistry (Zewail, 1994). In the photoexcited electronic state the interatomic potential changes and determines the motion of atomic wavepackets prepared by a femtosecond (fs) light pulse. This may induce drastic effects such as breaking of bonds and subsequent chemical transformation. More recently a new field has emerged within material science, whereby an ultra-short laser pulse may induce the collective and/or cooperative transformation of the material towards another macroscopic state which can be of different electronic and/or structural order (Nasu, 2004; Buron & Collet, 2005; Kuwata-Gonokami & Koshihara, 2006; Tanaka *et al.*, 2009). This can trigger spectacular switching of the physical properties of materials, for example from nonmagnetic to magnetic or from insulator to conductor. The goal is then to realize at the level of a material what femtochemistry has achieved at the level of a single molecule.

Materials with photoactive multifunctional molecules, which can switch between two states, are particularly promising to explore. Among these, spin-crossover compounds are prototypes of molecular bistability in the solid state. The molecules may be switched from low-spin (LS) to high-spin (HS) states under various external perturbations, including light irradiation (Gütlich & Goodwin, 2004). This switching leads to a change in magnetic and optical properties as well as a structural reorganization. Structural investigations of light-driven switching of spin-crossover solids have so far been limited to photostationary states at low temperature (Kusz *et al.*, 2001; Marchivie *et al.*, 2002; Huby *et al.*, 2004; Ichiyanagi *et al.*, 2006; Pillet *et al.*, 2006). Still, a central question remains about the determination of the dynamics of the photoswitching processes in these materials, since those investigations dealt mainly with the slow kinetics of recovery to the thermally stable state (Enachescu *et al.*, 2006; Fouché *et al.*, 2009), but not the phototransformation. In solids we can expect the photoinduced dynamics to follow a complex pathway from molecular to material scales through a sequence of processes. Time-resolved diffraction is a direct method of probing the structural dynamics of a material while they

happen, such as changes of molecular geometry, unit-cell volume and thermal motions (Cailleau *et al.*, 2004; Chergui & Zewail, 2009). This is feasible on time-resolved beamlines installed on third-generation synchrotron sources, the flux of which allows many Bragg peaks to be recorded by monochromatic X-ray diffraction with a time resolution of 100 ps (Techert *et al.*, 2001; Collet *et al.*, 2003, 2006, 2008; Cailleau *et al.*, 2004; Guérin *et al.*, 2004; Koshihara & Adachi, 2006; Nozawa *et al.*, 2007).

The aim of this contribution is to discuss such structural dynamics in molecular materials. In §2, we show how a time-resolved diffraction experiment captures the successive steps of the photoinduced switching dynamics in a spin-crossover solid. In §3 the physical picture of such a photoinduced transformation in a material is discussed.

2. Probing successive steps of the photoinduced switching dynamics in a spin-crossover material

In the solid state, the spin-crossover molecules may be switched from low-spin (LS) to high-spin (HS) states under various external perturbations, including light irradiation (Gütlich & Goodwin, 2004). This switching leads to a change in magnetic and optical properties as well as a structural reorganization. A central issue of the determination of the dynamics of the photoswitching processes in these materials has remained unsolved. In the literature, the photogeneration of molecules in solution to transient high-spin states has recently been reported and investigated by time-resolved X-ray spectroscopy (Khalil *et al.*, 2006; Gawelda *et al.*, 2006; Bressler *et al.*, 2009). A detailed study of the out-of-equilibrium switching dynamics triggered by a femtosecond laser flash was recently presented for the $[(TPA)Fe(TCC)]PF_6$ ferric catecholate spin-crossover crystal. The time-resolved X-ray diffraction and optical results show that the dynamics span from subpicosecond local photoswitching followed by volume expansion (nanosecond timescale) and thermal switching (microsecond timescale). Here we present complementary results of the analysis of this mechanism.

$[(TPA)Fe(TCC)]PF_6$ has a short relaxation time (∼1 ms) of the photoexcited state around the crossover temperature (Enachescu *et al.*, 2006), thereby enabling a time-resolved experiment with a repetition rate of 1 kHz. At thermal equilibrium, the change in magnetic state (Fig. 1*a*) is associated with a thermal crossover between the two possible distributions of the five electrons on the *d* orbitals of Fe^{3+}: the low-temperature state (LS, $S = 1/2$) and the high-temperature state (HS, $S = 5/2$; Floquet *et al.*, 2005; Collet *et al.*, 2009). As the Fe^{3+} ion is in a ligand field of nearly octahedral symmetry, the main structural signature is the variation of the Fe–ligand bonds, especially with the N atoms. The ⟨Fe—N⟩ bond length varies from $\langle Fe{-}N\rangle_{LS}$ = 1.967 (3) Å to $\langle Fe{-}N\rangle_{HS}$ = 2.127 (3) Å between the LS and HS states, respectively (Fig. 1*b*), as determined from structure refinements at thermal equilibrium (complete HS state at 400 K and LS state at 80 K; Collet *et al.*, 2009). As the thermal crossover (centered at the temperature $T_{1/2}$ = 214 K) takes place with a continuous evolution of the high-spin fraction from $X_{HS} = 1$ at high temperature to $X_{HS} = 0$ at low temperature, ⟨Fe—N⟩ also changes continuously, as a result of the statistical distribution of HS and LS molecular states over the crystalline sites. It was reported (Lorenc *et al.*, 2009) that the thermal evolution of ⟨Fe—N⟩ perfectly scales with the thermal evolution of X_{HS} through

$$\langle Fe{-}N\rangle(T) = X_{HS}(T)\langle Fe{-}N\rangle_{HS} + [1 - X_{HS}(T)]\langle Fe{-}N\rangle_{LS}. \quad (1)$$

The picosecond structural analysis performed on the time-resolved X-ray diffraction beamline ID09B at the ESRF (Lorenc *et al.*, 2009) demonstrated that the photoswitching spin-crossover dynamics are a multistep process. Three main steps were identified in the fs–µs transformation dynamics, and the recovery to the thermal equilibrium with the sample environment occurs on the microsecond timescale. The three steps are:

(i) the subpicosecond photoinduced molecular switching,
(ii) unit-cell volume expansion on a 10 ns timescale and
(iii) significant thermal effect on a µs timescale.

In the following subsections, after a description of the experimental setup, we present in detail these three steps and the microsecond relaxation process.

2.1. Picosecond pump–probe diffraction

Time-resolved X-ray diffraction is an established technique now and it is implemented at many synchrotron facilities. The present time-resolved diffraction experiments were performed at the ID09B beamline at ESRF (Wulff *et al.*, 2004, 2007;

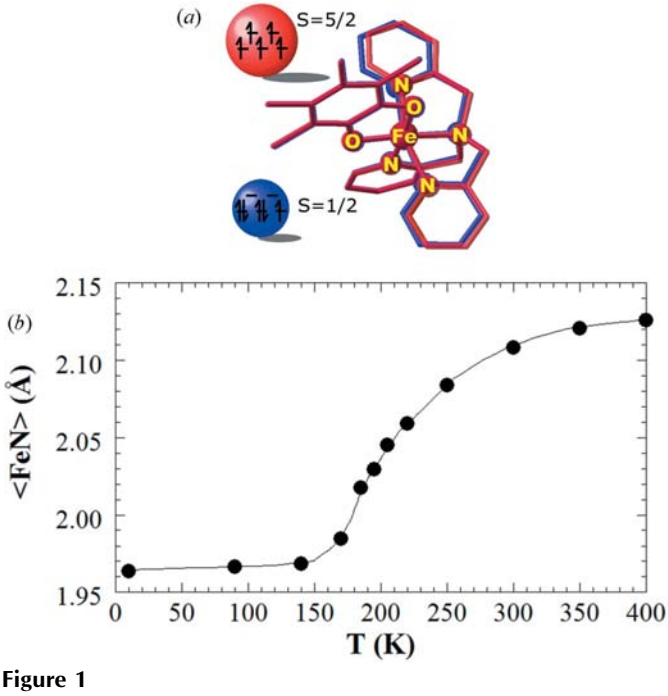

Figure 1
(*a*) The $[(TPA)Fe(TCC)]^+$ cation and the structural reorganization between the LS (blue) and HS (red) states. (*b*) Temperature dependence of the ⟨Fe—N⟩ bond length associated with the spin crossover.

Cammarata *et al.*, 2009). The 100 fs oscillator, phase-locked to the radio-frequency cavity of the synchrotron, seeds the regenerative/multipass amplifiers operating at ∼1 kHz, the 355th subharmonic of the orbit frequency of an electron bunch in the storage ring of the synchrotron. Polychromatic X-ray pulses of ∼100 ps duration with $\sim 10^9$ photons per pulse are delivered by the U17 in-vacuum undulator. The fundamental energy of U17 can be tuned between 15 and 20 keV where diffraction experiments have the best trade-off between detected intensity and radiation damage. The spectrum of the fundamental is quasi-monochromatic with a $\Delta E/E$ of 3%. This spectrum can be further monochromated with an Si(111) crystal to $\Delta E/E$ of 0.01% at the expense of flux, which goes down by a factor of ∼1000. This monochromatic beam is used for diffraction from molecular single crystals. One of the challenges in pump–probe experiments at synchrotrons is to control the pulse structure on the sample. In experiments with integrating charge-couple device (CCD) detectors the time resolution is assured by time gating the X-ray pulse to the laser pulse when both pulses arrive in pairs on the sample. The frequency of the 16-bunch mode, a common bunch-filling mode for time-resolved experiments, is 5.7 MHz, which is too fast for 1 kHz amplified laser systems (Cammarata *et al.*, 2009).

We probed the sample by recording the X-ray diffraction pattern stroboscopically at 994 Hz, as a function of the delay after photoexcitation with a 100 fs pulse at 800 nm (1.55 eV). Data reduction and lattice parameters were obtained using the software *Crysalis RED* (Oxford Diffraction, 2008) with $0.05 < R < 0.06$. The structures obtained in the stroboscopic mode were similar to those obtained at thermal equilibrium (Collet *et al.*, 2009). Different types of data-collection routines were performed: partial oscillations of 5 µm-thick plate-shaped crystals to accurately check the time dependence of the lattice parameter *a*, and the full oscillation of 10–15 µm-thick needle-shaped crystals to solve the structure and check molecular reorganizations. Simultaneous top and bottom illumination of the crystal was used to maximize the transformation rate (∼150 µJ mm^{-2}) as the penetration depth of the laser is ∼5 µm.

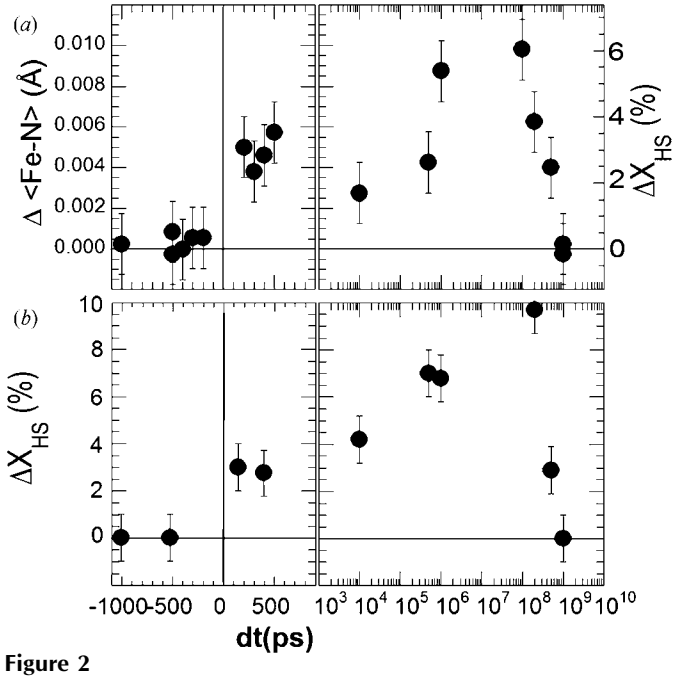

Figure 2
(*a*) Time-delay dependence of $\Delta\langle \mathrm{Fe-N}\rangle$, associated with the change of spin state and deduced variation of the HS molecular fraction, ΔX_{HS}. (*b*) Variation of the HS molecular fraction ΔX_{HS} as a function of the time delay, *dt*, between the laser pump and the X-ray probe deduced from the variation of the structure factors.

2.2. Picosecond photoinduced molecular switching

The photoinduced switching of the HS molecular state was shown over a plateau extending from 1 ps up to ns through the variation of the optical transmission of single crystals (Lorenc *et al.*, 2009), as well as from the variation of the $\langle \mathrm{Fe-N}\rangle$ average bond length obtained by the picosecond diffraction technique presented in Fig. 2. As shown in equation (1), $\langle \mathrm{Fe-N}\rangle$ is the weighted sum of the HS and LS average bond length. In the time domain, the temporal evolution of $\langle \mathrm{Fe-N}\rangle(t)$ depends on the temporal evolution of $X_{\mathrm{HS}}(t)$ according to

$$\langle \mathrm{Fe-N}\rangle(t) = X_{\mathrm{HS}}(t)\langle \mathrm{Fe-N}\rangle_{\mathrm{HS}} + [1 - X_{\mathrm{HS}}(t)]\langle \mathrm{Fe-N}\rangle_{\mathrm{LS}}. \quad (2)$$

The observed increase of $\langle \mathrm{Fe-N}\rangle$ is therefore due to an increased population of HS-state molecules generated by laser excitation. The variation of the fraction of HS molecules (ΔX_{HS}) was extracted from its time variation $\Delta\langle \mathrm{Fe-N}\rangle(t)$ according to

$$\Delta X_{\mathrm{HS}}(t) = \Delta\langle \mathrm{Fe-N}\rangle(t)/[\langle \mathrm{Fe-N}\rangle_{\mathrm{HS}} - \langle \mathrm{Fe-N}\rangle_{\mathrm{LS}}]. \quad (3)$$

Both parameters are presented in Fig. 2(*a*). ΔX_{HS} indicates an instantaneous increase of ∼3% of HS-state molecules just after the laser flash in the first 100 ps of the photo-transformation (time resolution of the experiment). Variations of X_{HS} compared with excitation densities used indicate that a single absorbed photon transforms a single molecule in the early stage and no cooperative effect could be detected.

Another way to obtain the change in the HS-state molecular fraction is to use the X-ray structure factors, F_{hkl}, deduced from the measurements of Bragg-peak intensities I_{hkl}. Indeed, as the crystal is a random mixture of HS- and LS-state molecules, the average X-ray structure factor can be expressed as a weighted sum of HS- and LS-state structure factors, $F_{hkl}(\mathrm{HS})$ and $F_{hkl}(\mathrm{LS})$, according to

$$\langle F_{hkl}(t)\rangle = X_{\mathrm{HS}}(t)F_{hkl}(\mathrm{HS}) + [1 - X_{\mathrm{HS}}(t)]F_{hkl}(\mathrm{LS}), \quad (4)$$

where *t* is the time delay. Values of $F_{hkl}(\mathrm{LS})$ and $F_{hkl}(\mathrm{HS})$ have been obtained from thermal equilibrium structure refinements at 80 and 400 K, where the fraction of HS states approaches 0 and 1, respectively (Collet *et al.*, 2009). As the difference between $F_{hkl}(400\ \mathrm{K})$ and $F_{hkl}(80\ \mathrm{K})$ is due in part to the temperature difference, an isotropic temperature factor difference, ΔB, has been extracted from the Wilson plot, as detailed in §2.4, according to the relation

$$I_{400\,\mathrm{K}}(q) = I_{80\,\mathrm{K}}(q)\exp(-\Delta B \cdot q^2), \quad (5)$$

where q is the reciprocal-lattice vector. Intensities measured at 400 K are then corrected for this temperature discrepancy effect before extracting the corresponding structure factors F_{hkl}(HS). Several data collections were been performed on the same crystal and we extracted the variation of the ratio of HS-state molecules, $\Delta X_{\rm HS}(t)$, by comparing thousands of Bragg reflections through the relation

$$\Delta X_{\rm HS}(t) = \frac{F_{hkl}(t) - F_{hkl}(dt<0)}{F_{hkl}({\rm HS}) - F_{hkl}({\rm LS})}, \qquad (6)$$

where $F_{hkl}(dt<0)$ is the average structure factor obtained with negative delays, *i.e.* before the laser irradiation. The results are presented in Fig. 2(*b*). Again, the observed time dependence of $\Delta X_{\rm HS}$ points to an instantaneous 3% increase 200 ps after the laser flash. The increase is even stronger around 100 µs, as it reaches 8–10%. By comparing with the values of $\Delta X_{\rm HS}(t)$ obtained from the variation of ⟨Fe−N⟩, both methods give the same qualitative picture: an instantaneous increase of HS-state molecules after the laser flash, followed by an amplification in the µs regime. The latter is due to a thermal heating effect, as detailed in §2.4. The accuracy of this last method is, however, limited by the approximation resulting from structure-factor corrections through the Debye–Waller factor, or the heating effects which occur after µs delays as discussed below.

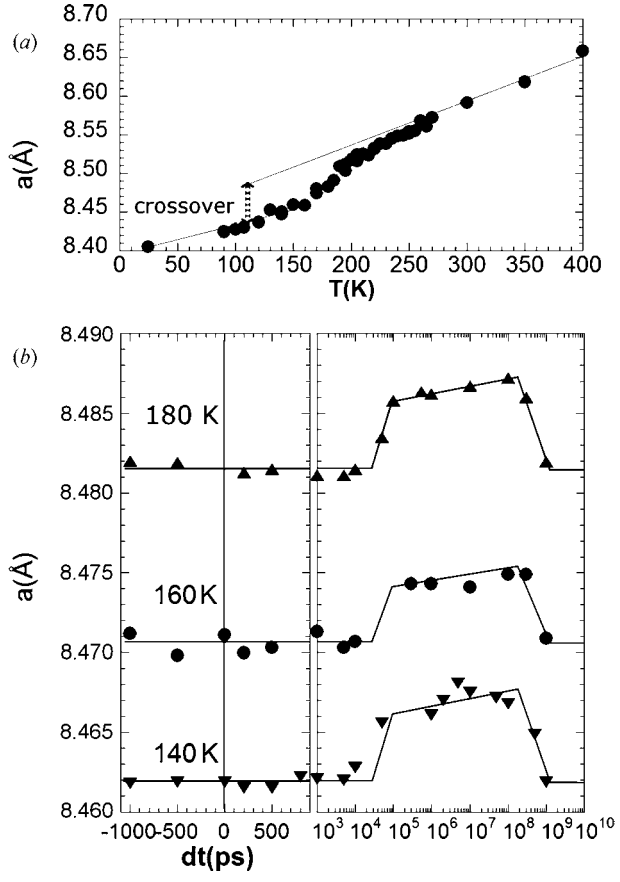

Figure 3
(*a*) Temperature dependence of the lattice parameter a at thermal equilibrium and (*b*) its time dependence during the photoinduced process, observed at different temperatures.

2.3. Nanosecond volume expansion

In spin-crossover complexes elastic effects play a key role because of the molecular expansion between LS and HS states. Therefore, as the temperature is changed, there are two contributions to the volume expansion: one is due to the thermal lattice expansion and the other one is due to the elastic effect as molecules switch from LS to HS states during the spin crossover. As most of the spin crossover takes place in the 160–220 K range, one can distinguish both contributions to the thermal dependence of the lattice parameter a plotted in Fig. 3(*a*).

During the photoswitching process, we observe that the lattice expansion is not instantaneous but is significantly delayed from the molecular structural reorganization. The lattice parameters expand only after a lapse of ∼50 ns, as shown in Fig. 3(*b*) for the parameter a at different temperatures (140, 160 and 180 K). The lapse corresponds to the time delay required for acoustic wave propagation (∼1000 m s^{-1}) in a thin crystal of a few tens of µm. In all cases, the first sharp increase of the lattice parameter (around 50 ns) is followed by a smoother expansion in the 100 ns to 100 µs regime, which may be due to the thermal processes discussed below.

2.4. Additional microsecond thermoswitching

The high energy deposited (∼1.5 eV) in comparison with the energy difference between LS and HS states (tens of meV) must result in some heat diffusion. As mentioned previously, it is possible to detect and estimate a temperature difference between two data collections by plotting Wilson graphs. These are based on the comparison of diffracted peak intensities. It is well known that the intensity of any Bragg peak decreases with increasing incoherent thermal vibrations around the average atomic positions. By assuming an overall increase of isotropic atomic motion ΔB associated with thermal heating, the intensity I_0 at a given temperature T_0 (taken as a reference) of the Bragg reflections is therefore decreased to I_1 at a higher temperature T_1 and $I_1(q) = I_0(q)\exp(-\Delta B \cdot q^2)$. The slope of the dependence of $\ln(I_1/I_0)$ with the square of the scattering vector q gives ΔB. Measuring ΔB therefore makes it possible to detect the heating effect through the associated increase of atomic thermal motion, as presented in Fig. 4 between 90 and 300 K. By comparing different data sets at different temperatures, we have observed that the slope ΔB is roughly proportional to the temperature difference.

In the time domain, Wilson graphs compare data sets at a given positive delay with a reference data set obtained with a negative delay (Figs. 4 and 5). We can conclude that global heating is not detectable over a short delay time. It only appears on the microsecond timescale. The comparison of the ΔB values obtained in the time domain with those obtained at thermal equilibrium allows us to estimate the corresponding temperature increase after µs delays to ∼40 K. This heating effect is the origin of the additional HS fraction conversion observed on the µs timescale (Fig. 2). The lattice parameter a continues to expand in the 100 ns to 100 µs regime (Fig. 3), which is related to the µs heating effect. By comparing the

global variation of 0.007 Å between the negative and µs regime a temperature increase of ∼10 K can be deduced, which is lower than the value deduced from ΔB. It is clear with both methods that a thermal heating occurs; however, its value is difficult to determine precisely. We demonstrated that two types of LS- to HS-state switching occur successively and are well separated in the time domain: a photoinduced conversion (ps timescale) and a thermoinduced one (µs timescale).

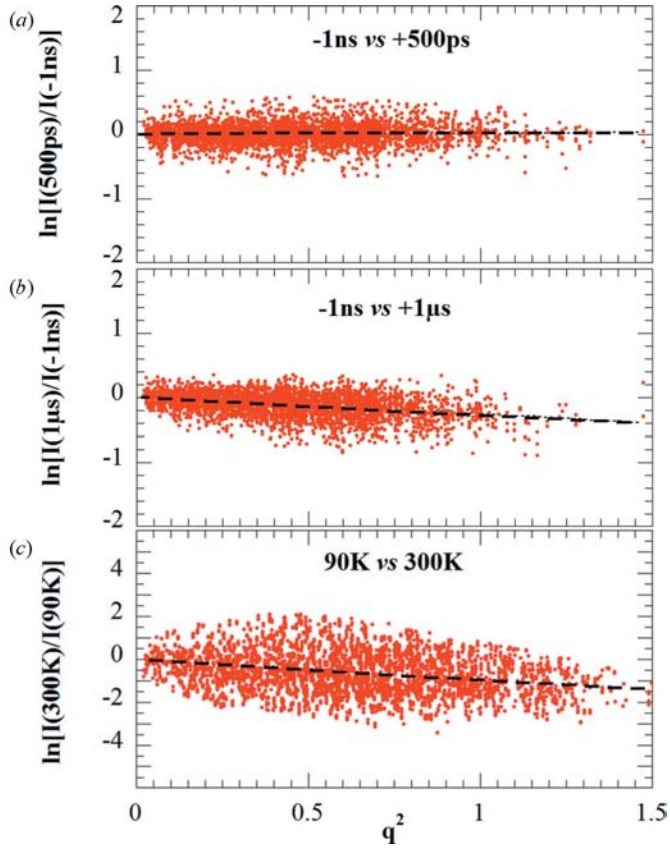

Figure 4
Wilson plots showing the variation of temperature with negative delay (T_0 = 180 K) and (*a*) 500 ps with $\Delta B = 0$; (*b*) 1 µs with $\Delta B \simeq 0.15$; and (*c*) between 90 and 300 K with $\Delta B \simeq 1$.

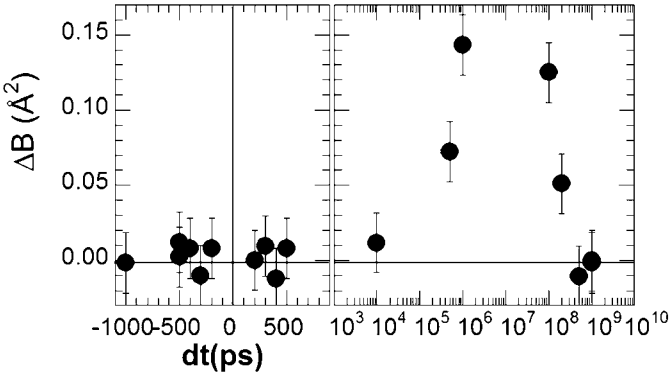

Figure 5
Time dependence of the isotropic thermal factor ΔB.

2.5. One-step millisecond relaxation

The millisecond relaxation process toward the ground states follows an exponential-like law, as evidenced by optical techniques (Enachescu *et al.*, 2006), as well as X-ray diffraction measurements presented here. Fig. 6 depicts the µs–ms relaxation of the ⟨Fe—N⟩ values as well as that of the lattice parameter *a*. The recovery to equilibrium occurs on a timescale of 100 µs to 1 ms, in agreement with optical investigations.

3. Physical picture of photoinduced molecular material switching

The femtoswitching of a molecular material, *i.e.* the switching of its macroscopic state induced by an ultra-short laser pulse, ensues the now established field of femtochemistry in solution where photochemical molecular processes are independent (Zewail, 1994). Indeed, in the solid state photoactive molecules interact and this may be at the origin of fascinating collective and cooperative phenomena. The properties of a solid in the ground state and at thermal equilibrium are generally well understood. Thus, atomic vibrations can be decomposed into normal collective modes extending over the crystal. In the same way, despite a large diversity of phenomena in systems of different nature, a universal description of phase transitions at thermal equilibrium has been established such as symmetry breaking, order parameter, Landau expansion of free energy *etc.* X-ray, neutron and electron scattering investigations have largely contributed to a global picture of collective excitations as well as structural changes in phase transitions at thermal equilibrium. Obviously, such a global picture for collective and cooperative non-equilibrium phenomena induced by a light pulse is missing. A new approach is required with the introduction of new conceptual tools. To progress along this direction we benefit from spectacular advances in pulsed X-ray and elec-

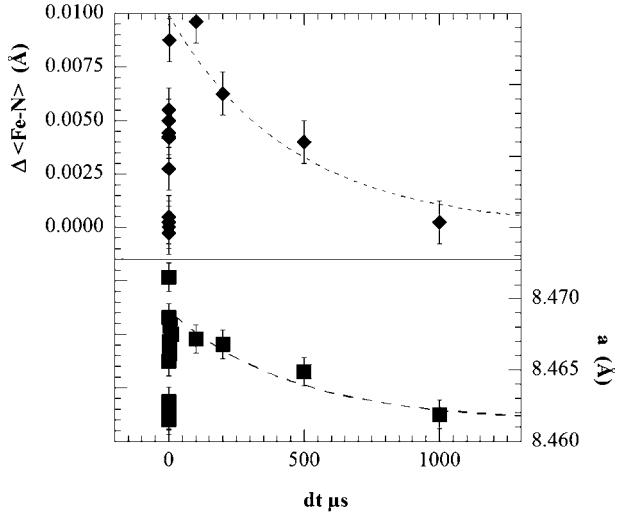

Figure 6
µs–ms relaxation of the ⟨Fe—N⟩ bond length and lattice parameter *a*.

tron sources to investigate fast and ultra-fast structural dynamics.

A universal concept to describe the stability, metastability and instability of a system and its subsequent dynamics or kinetics is that of a potential-energy landscape, such as a mechanic potential energy for particle motion, a potential-energy surface (PES) for chemical kinetics or a thermodynamic potential such as free energy for a phase transition at thermal equilibrium. For photoinduced phenomena in a material triggered by an ultra-short laser pulse the situation is less clear and it becomes riskier to make general statements. In fact, the pathway is complex for such macroscopic systems, which have a gigantic number of degrees of freedom in comparison to chemical transformation at the molecular level. The key point is that dynamical changes span over different length scales and timescales and are manifested by a sequence of processes, as illustrated by the results presented in §2. Indeed, in the solid state different subsystems of a different nature, such as electrons, spins, phonons, molecular configurations, unit-cell deformations and so on, play their part on different typical timescales. For instance, the electronic motion takes place on the fs timescale, while the atomic motion is on the ps timescale, in agreement with the increase of mass. Thus, in a given timescale for dynamics involving certain degrees of freedom, other degrees of freedom are either faster or slower, so they act by their statistical average or as frozen. Therefore, the description that works at one scale may be inappropriate at other scales. For a given step the adequate potential energy governing atomic motion or rearrangements is subordinated to the nature of parameters which remain constant during the corresponding range of timescale, since some degrees of freedom are frozen, for instance volume in an early stage. Furthermore, the potential-energy landscape defining the dynamics of the evolving degrees of freedom is driven by the quantum or thermal average of faster degrees of freedom. It spans from mechanic potential energy directing deterministic coherent dynamics to thermodynamic potential governing kinetics towards some equilibrium. The preceding step determines the new initial condition for the next step. For the first step the initial condition is determined by the physical state prepared by the laser pulse. In addition, feedback mechanisms driven by cooperative interactions bring some complexity to the different successive dynamical processes. However, we should stress that in some cases it may be difficult to clearly separate those different steps.

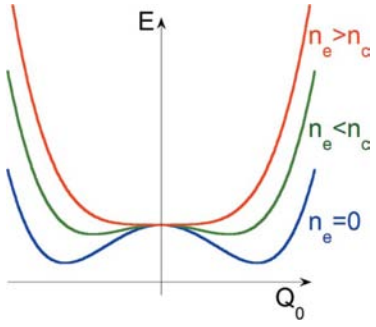

Figure 7
Schematic physical picture for the case of delocalized excitation. The energy potential governing the atomic motions is the electronic energy as a function of the collective normal coordinate (order parameter) and is shown for three different densities n_e of photoexcited electrons (control parameter) below and above the critical density n_c.

It is advisable to distinguish between the situation of delocalized and localized electronic excitation. Delocalized electronic excitation has been extensively studied and theoretical approaches have been reviewed in a recent paper focusing on itinerant electron systems (Yonemitsu & Nasu, 2008). Localized electronic excitation, corresponding to the case experimentally investigated here, has scarcely been studied.

3.1. Delocalized electronic excitation

As already mentioned, in femtochemistry an ultra-short light pulse prepares a coherent atomic wave packet for each excited molecule. This kind of coherent process may be extended to materials. In the case of delocalized electronic excitation it concerns collective degrees of freedom such as a coherent optical phonon mode triggering the oscillation of a long-range atomic order on a macroscopic scale. Bismuth exemplifies this situation for an itinerant electron system (Sokolowski-Tinten *et al.*, 2003; Fritz *et al.*, 2007). The thermalization of the electronic subsystem through strong electron–electron interaction is ultra-fast, in general on a timescale of the order of the duration of the light pulse. Then on the 10–100 fs timescale we can define an electronic temperature (depending on the fraction of excited electrons n_e) which can be very high, a few thousands of K, while atoms do not have time to move. The change of interatomic forces governed by the statistical average of the new electronic Fermi–Dirac distribution induces a deterministic and collective atomic oscillation around new equilibrium positions defined in the new potential (Fig. 7). For a short timescale with regard to the phonon–phonon relaxation time, often a few 10 ps, the collective oscillation mode can be considered as purely a mechanical system without entropy and the process is isentropic, *i.e.* at constant electronic entropy. It exhibits a simultaneous oscillation of the electronic temperature (Stampfli & Bennemann, 1990; Zijlstra *et al.*, 2006). This behavior is analogous to the oscillation of a piston for a small friction force when the applied force compressing a gas is suddenly removed. What we want to point out is that the relevant mechanic PES is that of the electronic energy at constant entropy as a function of normal coordinates and this constitutes a nice extension of the Born–Oppenheimer approximation, as Stampfli & Bennemann (1990) discussed some time ago. For a high density of photoexcited electrons the process becomes nonlinear and this can lead to the appearance of lattice instability at the critical value n_c. According to Landau's description of the structural phase transition at thermal equilibrium, the relevant collective normal coordinate is always the order parameter (Fig. 7). However, the control parameter is no longer the temperature but this initial density of photoexcited electrons.

3.2. Electronic excitation localized at the molecular level

The situation is intrinsically different in the case of the photoexcitation of localized electrons on molecules in a material. Indeed, on an ultra-short timescale (subpicosecond), in agreement with a typical period of intramolecular vibrations, the molecular relaxation of the local excited state manifests itself by intramolecular reorganization (Fig. 8). In the present case, it is for instance the significant elongation of the metal–ligand bond length from the LS to HS state in a spin-crossover molecule (Moisan *et al.*, 2008; Lorenc *et al.*, 2009). Notice that the intramolecular structural relaxation takes place on a similar timescale to that for molecules in solution (Bressler *et al.*, 2009). It gives rise to an energy barrier between the trapped molecular excited state and the ground state, leading to a stabilization of the photoswitched molecular state over a much longer time (Fig. 8). The rate constants of the corresponding thermally activated processes were obtained for a series of similar Fe(III) solids to that studied in §2 (Enachescu *et al.*, 2006). From there we estimate that a relative LS/HS population becomes thermally equilibrated with the lattice in a time of the order of μs at a temperature around $T_{1/2}$, and probably more in many other spin-crossover systems, in particular Fe(II) ones. In other words, in the submicrosecond timescale the solid can be considered as being composed of 'hot' molecules dispersed in a cold lattice, by comparison with the 'hot' collective coherent phonon mode in the delocalized situation discussed previously. 'Hot' (in quotes) is used for simplicity, as the concept of temperature is meaningless at the level of a single molecule or a single collective mode. It is not possible either to consider an electronic temperature in this localized situation. Furthermore, the non-radiative energy dissipation of relaxing molecular excited states heats the lattice. Note that for a spin-crossover compound the absorbed optical energy ($\simeq$ 1.55 eV) is much higher than the energy difference between HS and LS states (a few tens of meV). Two kinds of pertinent degrees of freedom have to be considered. On the one hand there are the configuration arrangements (σ) described by a pseudo-spin variable σ_i to characterize the two molecular states on each site i: $\sigma_i = +1$ for HS and -1 for LS. On the other hand, there are the vibration states (υ), referred to as the lattice subsystem. They exhibit a very different typical timescale since the thermalization of vibration modes in general occurs on the picosecond scale, while the configuration arrangements are governed by slow thermally activated dynamics. We can stress that this was actually taken into account in the mapping by an Ising-like model of thermal transformation of a spin-crossover solid where the field term is temperature dependent (Boukheddaden *et al.*, 2000). Indeed fast electronic and vibration degrees of freedom are integrated to obtain an effective Ising-like Hamiltonian for the slower HS–LS configuration degrees of freedom, thereby including the entropic effect of electronic multiplicity and vibration in the field term.

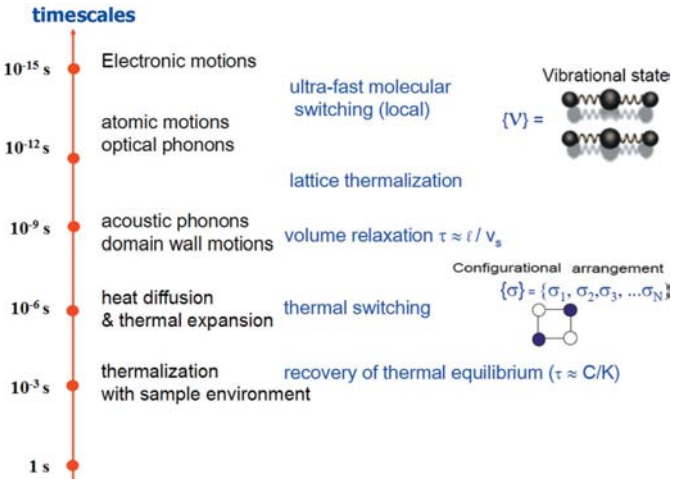

Figure 8
Timescales of consecutive dynamic processes for photoinduced molecular switching in the solid state.

3.3. Volume expansion

An essential feature to take into account during the photoinduced transformation of a material is the dynamical process of volume expansion and crystal deformation. These concern macroscopic dimensions, which require a movement of the atoms or molecules over long distances. It involves propagation of cell distortion inside the irradiated part of the crystal limited by a speed similar to that of sound (a few thousands of m per s). It corresponds to the nanosecond range for a distance of a few micrometres (Fig. 8). Then in the first step the unit cell does not distort. Only the reorganization of atoms associated with relative displacements inside the cell takes place. This corresponds to a transformation at constant volume, where the crystal is isolated without exchange of work and heat with the environment. During the subpicosecond timescale some deterministic nonthermal atomic motions can occur, as is nicely illustrated by the observation of coherent optical phonon modes discussed above. The thermalization of the lattice subsystem owing to phonon–phonon interaction follows, typically in the range of tens of picoseconds, and causes an increase of internal pressure (or more generally stress). The pressure is released by the volume expansion on a longer timescale. This agrees with our observation in the spin-crossover system under consideration in §2.3. In the same way a shear deformation arising at 100 ps for a length scale of hundreds of nanometres has been reported for the itinerant electron system of vanadium dioxide (Baum *et al.*, 2007). Note that the volume expansion has to be considered both for the parallel and perpendicular directions of the surface irradiated by the laser beam.

It is useful to make the following remarks. Firstly, regarding the origin of volume expansion, in addition to the effect of the lattice temperature increase we have to consider the coupling between the cell deformation and the order parameter in the case where a photoinduced phase transition occurs. At thermal equilibrium the effect of this coupling is well known, and the establishment of the new (quasi-)equilibrium phase

manifests itself by a more or less important change of the unit cell. In a similar way the photoinduced phase transition effect adds or subtracts to that of temperature increase. Such a phase transition feature is particularly illustrative in a ferroelastic situation, as shown by the above-mentioned shear deformation (Baum *et al.*, 2007). Even when a phase transition does not take place, as in the spin-crossover system investigated here, since it exhibits a gradual change characteristic of a situation above a critical point, some other origin of lattice expansion than lattice temperature increase can manifest itself. Thus, in such a spin-crossover system elastic interaction resulting from swelling of phototransformed HS molecules is another possible cause for volume expansion. Furthermore, a self-amplification of the number of switched molecules is expected in a more cooperative system than the present case. This will be associated with the propagation of a phase front (Okimoto *et al.*, 2009). Such behavior underlines the active role of silent molecules in the bulk solid, which is intrinsically different from molecules in solution. Nonetheless, induced thermal expansion has also been clearly observed in solution under similar experimental conditions (Wulff *et al.*, 2006). We expect this dynamical process will fundamentally change in nature and timescale for nanoparticles.

3.4. Heat diffusion

Another physical problem to discuss is the slow heat diffusion through the sample to restore temperature homogeneity. Owing to the finite penetration depth, which depends on the excitation wavelength and varies from submicrometre to a few micrometres, the pump laser causes gradients of deposited energy and thus of local temperature. The time required to homogenize temperature across the crystal is governed by heat diffusivity with typical values of the order 10^{-6} m^2 s^{-1} and corresponds to the microsecond range for a micrometre length scale (Fig. 8). The significant increase of an isotropic temperature factor reported in §2 is a good illustration of this physical feature. Notice the nonlinear increase of internal energy with temperature, contrary to a classical perfect gas or oscillator, is at the origin of the increase of average temperature with respect to the inhomogeneous state. This also manifests itself by a significant increase of switched molecules, illustrating again the active role of silent molecules in a material.

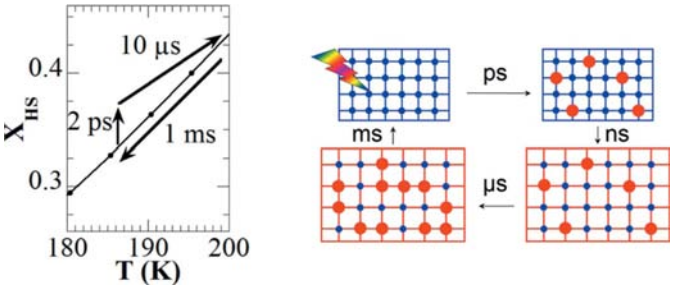

Figure 9
Schematic drawing of the structural dynamics of molecular switching in the solid state induced by a fs laser flash.

3.5. Recovery to thermal equilibrium with sample environment

Finally, we can say something about the recovery to thermal equilibrium with sample environment (cryostat). If the investigated sample achieves its thermal equilibrium on the µs timescale, typical for thermally activated switching and temperature homogenization, no heat transfer with the sample environment has yet taken place. The equilibration time is governed by sample–environment heat transfer, more quantitatively by the ratio between the sample heat capacity and the heat-transfer rate between the sample surface and the cryogenic flow. It then increases with sample size. For a size of a few hundred micrometres we consider the equilibration to be efficient only for a few hundred microseconds (Fig. 8). In fact, a laser repetition rate of 1 kHz is truly the limit for such large samples. Note that in the situation of a suspension of nanoparticles the heat transfer with the liquid environment will be very fast, which points to the interest these systems increasingly draw. We also have to stress that for a higher energy barrier and/or lower temperature, the thermally activated switching becomes slower than equilibration with the sample environment. The thermal equilibration with the sample environment is governed by stochastic dynamics which are much longer than those of more elementary physical processes (molecular and unit-cell deformations). These are therefore hidden in a statistical average. The elementary processes are only resolved during the phototransformation since they are clocked by the ultra-short laser pulse, as evidenced here with pump–probe methods.

4. Conclusion

Time-resolved diffraction is an excellent tool for directly observing the structural dynamics of a material rearrangement during the transformation induced by an ultra-short laser pulse. This is illustrated here with the dynamics of photoinduced molecular switching in the solid state probed by 100 ps X-ray diffraction. This time-resolved structural information is crucial for establishing the physical foundations of how to control macroscopic photoswitching in materials. A key feature is that the dynamics follow a complex pathway from molecular to material scale through a sequence of processes (Fig. 9). The solid is composed of subsystems different in nature with a macroscopic number of degrees of freedom (electrons, spins, phonons, molecular configuration, unit-cell deformation *etc.*). Not only is the pathway indirect, the nature of dynamical processes along the pathway depends on timescale. Indeed, this dictates which degrees of freedom are involved in the subsequent dynamics or kinetics and which are frozen or statistically averaged. On the one hand, this shows that the current situation is intrinsically more complex than a chemical reaction described in terms of a PES. It differs in many ways, and the valid description will not be a simple extension of a PES. Unlike independent photochemical process in solution, the solid medium is no longer passive but active, as illustrated here by the successive switching of silent

molecules in the material. On the other hand, it will be very fruitful to extend the universal tool used to describe phase transitions at thermal equilibrium to such cooperative dynamics far away from equilibrium. For instance, the Landau expansion of free energy taking into account the coupling between the order parameter and other parameters such as cell deformation is well established and its extension to the temporal domain is a fascinating goal. Furthermore, the observation of precursor cooperative phenomena owing to the formation of nanoscale clusters during some coherent nucleation and growth process (Ishida & Nasu, 2008*a*,*b*), which are the counterparts of the soft-mode mechanism in the case of delocalized electronic excitation, requires extending the ultra-fast X-ray techniques to time-resolved diffuse and small-angle scattering. Strong cooperative effects can be expected in systems presenting an abrupt transition at thermal equilibrium and may lead to phase coexistence. This situation will no longer allow averaging of the structure factor, but the intensities of the Bragg peaks of both phases, which superpose at constant volume and may split in reciprocal space as volume expansion occurs.

This work was supported by the Ministry of Research of France (ANR NT09-3-548342), Région Bretagne (CREATE Ultimate 4146, PRIR Femtocom 2178), Rennes Métropole and the Institut Universitaire de France. The authors are grateful to Marie-Laure Boillot, Shin-ya Koshihara and Michael Wulff for development of materials, experimental techniques and concepts.

References

Baum, P., Yang, D. S. & Zewail, A. H. (2007). *Science*, **318**, 788–792.

Boukheddaden, K., Sheto, I., Hôo, B. & Varret, F. (2000). *Phys. Rev. B*, **62**, 14796–14805.

Bressler, Ch., Milne, C., Pham, V.-T., ElNahhas, A., van der Veen, R. M., Gawelda, W., Johnson, S., Beaud, P., Grolimund, D., Kaiser, M., Borca, C. N., Ingold, G., Abela, R. & Chergui, M. (2009). *Science*, **323**, 489–492.

Buron, M. & Collet, E. (2005). Editors. *Second International Conference on Photoinduced Phase Transitions. J. Phys. Conf. Series*, Vol. 21.

Cailleau, H., Collet, E., Buron-Le Cointe, M. & Lemée-Cailleau, M. H. (2004). *Photoinduced Phase Transitions*, edited by K. Nasu, pp. 309–342. Singapore: World Scientific.

Cammarata, M., Eybert, L., Ewald, F., Reichenbach, W., Wulff, M., Anfinrund, P., Schotte, F., Plech, A., Kong, Q., Lorenc, M., Lindenau, B., Raebiger, J. & Polachowski, S. (2009). *Rev. Sci. Instrum.* **80**, 015101.

Chergui, M. & Zewail, A. H. (2009). *ChemPhysChem*, **10**, 28–43.

Collet, E., Boillot, M.-L., Hebert, J., Moisan, N., Servol, M., Lorenc, M., Toupet, L., Buron-Le Cointe, M., Tissot, A. & Sainton, J. (2009). *Acta Cryst.* B**65**, 474–480.

Collet, E., Buron-Le Cointe, M. & Cailleau, H. (2006). *J. Phys. Soc. Jpn*, **75**, 011002.

Collet, E., Buron-Le Cointe, M., Lorenc, M. & Cailleau, H. (2008). *Z. Kristallogr.* **223**, 272–282.

Collet, E., Lemée-Cailleau, M. H., Buron-Le Cointe, M., Cailleau, H., Wulff, M., Luty, T., Koshihara, S., Meyer, M., Toupet, L., Rabiller, P. & Techert, S. (2003). *Science*, **300**, 612–615.

Enachescu, C., Hauser, A., Girerd, J. J. & Boillot, M. L. (2006). *ChemPhysChem*, **7**, 1127–1135.

Floquet, S., Simaan, A. J., Rivière, E., Nierlich, M., Thuéry, P., Ensling, J., Gütlich, P., Girerd, J.-J. & Boillot, M.-L. (2005). *Dalton Trans*. pp. 1734–1742.

Fouché, O., Degert, J., Jonusauskas, G., Baldé, C., Desplanches, C., Létard, J. F. & Freysz, E. (2009). *Chem. Phys. Lett.* **469**, 274–278.

Fritz, D. M. *et al.* (2007). *Science*, **315**, 633–636.

Gawelda, W., Johnson, M., de Groot, F. M. F., Abela, R., Bressler, C. & Chergui, M. (2006). *J. Am. Chem. Soc.* **128**, 5001–5009.

Guérin, L., Collet, E., Lemée-Cailleau, M. H., Buron-Le Cointe, M., Cailleau, H., Plech, A., Wulff, M., Koshihara, S. & Luty, T. (2004). *Chem. Phys.* **299**, 163–170.

Gütlich, P. & Goodwin, H. A. (2004). Editors. *Spin Crossover in Transition Metal Compounds*, Vols. 233–235. New York: Springer.

Huby, N., Guérin, L., Collet, E., Toupet, L., Ameline, J. C., Cailleau, H., Roisnel, T., Tayagaki, T. & Tanaka, K. (2004). *Phys. Rev. B*, **69**, 020101(R).

Ichiyanagi, K., Hébert, J., Toupet, L., Cailleau, H., Guionneau, P., Létard, J. F. & Collet, E. (2006). *Phys. Rev. B*, **73**, 060408(R).

Ishida, K. & Nasu, K. (2008*a*). *Phys. Rev. Lett.* **100**, 116403.

Ishida, K. & Nasu, K. (2008*b*). *Phys. Rev. B*, **77**, 241303.

Khalil, M., Marcus, M. A., Smeigh, A. L., McCusker, J. K., Chong, H. H. W. & Schoenlein, R. W. (2006). *J. Phys. Chem. A*, **110**, 38–44.

Koshihara, S. & Adachi, S. (2006). *J. Phys. Soc. Jpn*, **75**, 011005.

Kusz, J., Spiering, H. & Gütlich, P. (2001). *J. Appl. Cryst.* **34**, 229–238.

Kuwata-Gonokami, M. & Koshihara, S. (2006). *J. Phys. Soc. Jpn*, **75**, 011001–011008.

Lorenc, M., Hébert, J., Moisan, N., Trzop, E., Servol, M., Buron-Le Cointe, M., Cailleau, H., Boillot, M. L., Pontecorvo, E., Wulff, M., Koshihara, S. & Collet, E. (2009). *Phys. Rev. Lett.* **103**, 028301.

Marchivie, M., Guionneau, P., Howard, J. A. K., Chastanet, G., Létard, J. F., Goeta, A. E. & Chasseau, D. (2002). *J. Am. Chem. Soc.* **124**, 194–195.

Moisan, N., Servol, M., Lorenc, M., Tissot, A., Boillot, M. L., Cailleau, H., Koshihara, S. & Collet, E. (2008). *C. R. Chim.* **11**, 1235–1240.

Nasu, K. (2004). Editor. *Photoinduced Phase Transitions*. Singapore: World Scientific.

Nozawa, S. *et al.* (2007). *J. Synchrotron Rad.* **14**, 313–319.

Okimoto, Y., Peng, X., Tamura, M., Morita, T., Onda, K., Ishikawa, T., Koshihara, S., Todoroki, N., Kyomen, T. & Itoh, M. (2009). *Phys. Rev. Lett.* **103**, 027402.

Oxford Diffraction (2008). *CrysAlis RED*, Version 1.171.26. Oxford Diffraction Ltd, Abingdon, Oxfordshire, England.

Pillet, S., Legrand, V., Souhassou, M. & Lecomte, C. (2006). *Phys. Rev. B*, **74**, 140101.

Sokolowski-Tinten, K., Blome, C., Blums, J., Cavalleri, A., Dietrich, C., Tarasevitch, A., Uschmann, I., Förster, E., Kammler, M., Horn-von-Hoegen, M. & von der Linde, D. (2003). *Nature (London)*, **422**, 287–289.

Stampfli, P. & Bennemann, K. H. (1990). *Phys. Rev. B*, **42**, 7163–7173.

Tanaka, K., Ogawa, T., Hashimoto, H. & Koshihara, S. (2009). Editors. *The LXII Yamada Conference on Photo-induced Phase Transitions and Cooperative Phenomena (PIPT3). J. Phys. Conf. Ser.* Vol. 149.

Techert, S., Schotte, F. & Wulff, M. (2001). *Phys. Rev. Lett.* **86**, 2030–2033.

Wulff, M., Bratos, S., Plech, A., Vuilleumier, R., Mirloup, F., Lorenc, M., Kong, Q. & Ihee, H. (2006). *J. Chem. Phys.* **124**, 034501.

Wulff, M., Kong, Q., Cammarata, M., Lo Russo, M., Anfinrud, P., Schotte, F., Lorenc, M., Ihee, H., Kim, T. K. & Plech, A. (2007). *AIP Conf. Proc.* **879**, 1187–1194.

Wulff, M., Lorenc, M., Plech, A., Ihee, H., Bratos, S., Mirloup, F. & Vuilleumier, R. (2004). *Femtochemistry and Femtobiology*, edited by M. M. Martin & J. T. Hynes, pp. 337–349. Amsterdam: Elsevier.

Yonemitsu, K. & Nasu, K. (2008). *Phys. Rep.* **465**, 1–60.

Zewail, A. (1994). *Femtochemistry: Ultrafast Dynamics of the Chemical Bond*, Vols. 1 and 2. Singapore: World Scientific.

Zijlstra, E. S., Tatarinova, L. L. & Garcia, M. E. (2006). *Phys. Rev. B*, **74**, 220301(R).